


Coupling effect of vibrations and residual electrostatic force in short-range gravitational experiments

Wen-Can Dong¹, Wen-Hai Tan², Zheng-Jie An², Hao Huang¹, Lin Zhu¹, Yu-Jie Tan¹,
Teng-Yu Long², Cheng-Gang Shao¹ and Shan-Qing Yang^{2,*}

¹MOE Key Laboratory of Fundamental Physical Quantities Measurement, Hubei Key Laboratory of Gravitation and Quantum Physics, PGMF and School of Physics, Huazhong University of Science and Technology, Wuhan 430074, People's Republic of China

²MOE Key Laboratory of TianQin Mission, TianQin Research Center for Gravitational Physics & School of Physics and Astronomy, Frontiers Science Center for TianQin, Gravitational Wave Research Center of CNSA, Sun Yat-sen University (Zhuhai Campus), Zhuhai 519082, People's Republic of China

 (Received 9 August 2023; revised 6 October 2023; accepted 2 November 2023; published 21 November 2023)

In the short-range test of the gravitational inverse-square law (ISL) using a torsion pendulum, the residual electrostatic force is usually the major disturbance. We have built a torsion pendulum apparatus to verify the coupling effect of the residual electrostatic force with the separation variation between the test mass and the shielding membrane due to the environmental vibrations. We present an alternative solution for reducing the disturbance by suspending the shielding membrane, which has a common mode response as the torsion pendulum to the seismic translational motion and ground tilt. The experimental results with a fixed membrane are in good agreement with the theoretical calculations. By replacing the fixed membrane with a suspended membrane, the sensitivity of the torsion pendulum has been improved by at least a factor of 3 from 0.5 to 20 mHz, which is very useful for the further improvement of the ISL test in short range. This work may be helpful for other small-force measurement experiments.

DOI: [10.1103/PhysRevApplied.20.054046](https://doi.org/10.1103/PhysRevApplied.20.054046)

I. INTRODUCTION

Theories that unify the four known fundamental interactions predict violations of the gravitational inverse-square law (ISL) at the laboratory length scale [1–8], providing strong motivation for testing the basic law of gravitation. The test of the ISL at length scales ranging from tens of microns to several centimeters are usually performed by using the torsion pendulum due to its high sensitivity to the horizontal force [9–17].

In these experiments, a conducting membrane is usually inserted between the test mass (the torsion pendulum) and the source mass to avoid direct electrostatic coupling when the position of the source mass is modulated periodically. Although most of the direct electrostatic force between the test and source masses is suppressed, the residual electrostatic interaction due to the patch effect and the contact potential difference between the test mass and the membrane is still the dominant noise [15–21]. The electrostatic effect has been extensively explored in the Casimir force measurements [22–32] and the gravitational wave detectors such as LIGO [33–36], LISA [37–40].

To reduce the electrostatic effect due to the nonzero potential difference between the pendulum and the

membrane, a strict separation stability is required. Usually in these experiments, the test mass is suspended by a long fiber, while the membrane is fixed to the vacuum chamber. This causes them to have different responses to the environmental vibration. As a result, the small separation fluctuations appear between the pendulum and the membrane, which can cause significant electrostatic force noise that far exceeds the sensitivity limit of the torsion pendulum. It has been found that the coupling of the vibration to the residual electrostatic force prevents improved testing of the alternative interaction at shorter separations [15–17], and must be suppressed.

In this paper, inspired by the work in Ref. [41], we present another solution for resolving the vibration disturbance in the short-range test of the ISL by suspending the shielding membrane, which has a common mode response as the torsion pendulum to the environmental vibration. We performed a comparison experiment to verify the common-mode suppression effect by using a fixed and a suspended membrane, respectively. The results show the effectiveness of the improvement.

II. EXPERIMENTAL SETUP

The schematic drawing of the experimental setup with a suspended membrane is shown in Fig. 1. An l-shaped torsion pendulum with total mass of 13 g was suspended by an

*yshq@mail.sysu.edu.cn

82-mm-long, 25- μm -diameter tungsten fiber. The torsion pendulum was made of two $20 \times 5 \times 5 \text{ mm}^3$ glass blocks and one $90 \times 8 \times 5 \text{ mm}^3$ glass block. The twist angle of the torsion pendulum was monitored by an autocollimator and controlled at a fixed position by two capacitive actuators using a proportional-integral-differential (PID) algorithm. A $20 \times 20 \times 0.005 \text{ mm}^3$ shielding membrane, with a surface flatness of $\pm 2.5 \mu\text{m}$, was tightly stretched and glued to a copper frame with a $10 \times 10 \text{ mm}^2$ square hole in the center. The copper frame was suspended by two 50-mm-long, 50- μm -diameter tungsten fibers to provide common-mode suppression for the pendulum-membrane separation variation due to the environmental vibration, but also to suppress the torsional motion. The pendulum and the membrane were each suspended under two magnetic dampers to further suppress their swing-mode motions. The damper with the torsion pendulum was connected to a rotary stage to adjust its equilibrium position, while another damper was connected to a translational stage to adjust the pendulum-membrane separation. The pendulum and the membrane were aligned to achieve the smallest possible separation.

The pendulum and the membrane were both gold coated to decrease the surface potential difference. While the pendulum was grounded, a high-precision voltage source meter was used to compensate the average surface potential on the membrane during each data run for further reducing the residual electrostatic interaction.

To suppress the influence of temperature variations, both the pendulum and the membrane were suspended from a Invar alloy frame with a low coefficient of thermal expansion. The entire system was installed in a vacuum chamber maintained at a pressure of approximately $5 \times 10^{-6} \text{ Pa}$ by an ion pump, which also provides thermal shielding from the atmospheric environment. The chamber was surrounded by a thermal shielding house consisting of several 2-mm-thick aluminum plates and 20-mm-thick foam boards to further reduce the temperature fluctuations and the airflow disturbances around the autocollimator.

To calibrate the sensitivity of the closed-loop pendulum, a copper cylinder mounted on a turntable outside the chamber was synchronously rotated to produce a calibrating gravitational torque. This torque was first determined through the free oscillation mode of the torsion pendulum at the pendulum-membrane separations larger than 2 mm for neglecting the residual electrostatic force [13–15].

In the vacuum of less than 10^{-5} Pa , considering the internal damping of the suspension fiber, the equation of motion of the torsion pendulum in closed-loop mode is

$$I\ddot{\theta} + (k - k_e + ik/Q)\theta = \tau_{\text{ext}} - \beta U_{\text{PID}}, \quad (1)$$

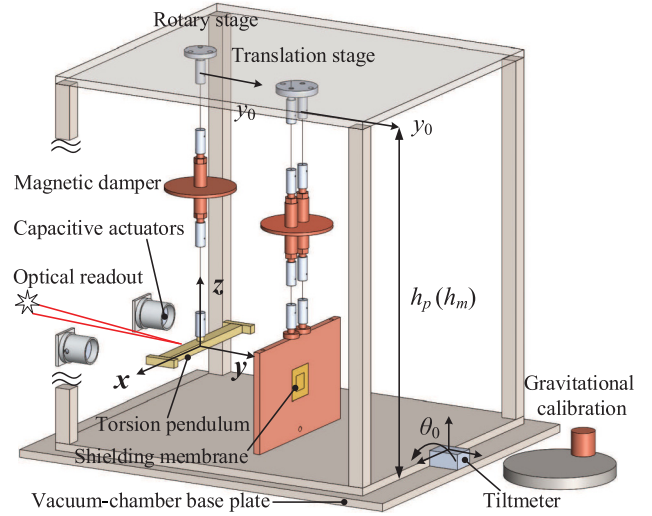


FIG. 1. Schematic drawing of the experimental setup (not to scale). The magnetic damper of the torsion pendulum and the shielding membrane were suspended from a rotary stage and a translation stage, respectively. The two stages were mounted on an Invar alloy frame fixed to the vacuum-chamber base plate. The translational motion of the suspension points y_0 and the tilt of the vacuum chamber θ_0 are also shown. The heights of the suspension points for the pendulum and the membrane relative to the base plate are h_p and h_m , respectively. The twist angle of the pendulum is measured by an autocollimator and controlled by two differential capacitive actuators. The sensitivity of the closed-loop pendulum is synchronously calibrated by a rotated copper cylinder outside the vacuum chamber.

where k_e is the electrostatic stiffness due to the residual potential difference with the membrane, τ_{ext} is the total external torque, k and Q are the spring constant and quality factor of the fiber, I is the moment of inertia of the pendulum, β is the ratio of the feedback torque to the feedback voltage U_{PID} , which is calculated as $U_{\text{PID}}(t) = k_p \theta(t) + k_d \dot{\theta}(t) + k_i \int \theta(t) dt$ according to the PID algorithm. The PID algorithm parameters k_p , k_i , k_d represent the proportional, integral, and differential term, respectively. The transfer function from the feedback voltage $U_{\text{PID}}(\omega)$ to the measured torque $\tau(\omega)$ is derived from Eq. (1) as

$$\begin{aligned} H_U(\omega) &\equiv \frac{U_{\text{PID}}(\omega)}{\tau(\omega)} \\ &= \frac{[k_p + \frac{k_i}{i\omega} + i\omega k_d] e^{-i\omega \Delta t}}{(k - k_e - I\omega^2) + i\frac{k}{Q} + \beta[k_p + \frac{k_i}{i\omega} + i\omega k_d] e^{-i\omega \Delta t}}, \end{aligned} \quad (2)$$

where $\Delta t = 1 \text{ s}$ is sampling interval, and $e^{-i\omega \Delta t}$ is the correction for the delay between the input and the output signal. The torque power spectrum density (PSD) of the torsion pendulum at small separation is $S_\tau^{1/2}(\omega) =$

$S_{U_{\text{PID}}}^{1/2}(\omega)/H_U(\omega)$. For the closed-loop pendulum at short range, the residual electrostatic stiffness k_e is determined by the response of the feedback voltage $U_c(\omega_c)$ to the known gravitational calibration signal $\tau_c(\omega_c)$, according to Eq. (2), namely $|H_U(\omega_c)| = |U_c(\omega_c)|/|\tau_c(\omega_c)|$ [16].

III. THEORETICAL CALCULATION OF ELECTROSTATIC TORQUE NOISE COUPLED TO THE ENVIRONMENTAL VIBRATION

In the ISL experiment, the electrostatic torque acting on the torsion pendulum can be expressed as

$$\tau_e = -\frac{L\epsilon_0 A}{2s^2} \Delta U^2, \quad (3)$$

where ϵ_0 is the vacuum dielectric constant, s is the pendulum-membrane separation, ΔU is the residual surface potential difference between the pendulum and the membrane, $L = 47.5$ mm and $A = 25$ mm² are the arm length of the pendulum and the facing area, respectively.

The electrostatic torque disturbance due to the tiny separation variation δs derived from Eq. (3) is

$$\delta\tau_e^s \equiv \frac{\partial\tau_e}{\partial s} \delta s = \frac{k_e}{L} \delta s. \quad (4)$$

This disturbance torque is proportional to δs with the scale factor k_e/L , where the electrostatic stiffness k_e can be calculated by the known gravitational source τ_c , so we focus on the theoretical calculation of δs , which may be caused by the environmental vibration of the seismic translational motion and ground-tilt noise.

We use a two-stage pendulum model to analyze the pendulum motions responding to the horizontal vibrations. The schematic diagram is shown in Fig. 2. The motions of the suspension point y_0^p and y_0^m relative to the inertial coordinate system $O - XYZ$ are considered as the input vibration noises. The variation of the separation $\Delta s = y_4^m - y_4^p$ will affect the residual electrostatic torque noise, and y_4^p and y_4^m are calculated independently while driven by the same environmental vibrations. For the subsystem including the torsion pendulum and that including the shielding membrane, the equation of motion of the two-stage pendulum system is given by

$$\begin{aligned} \theta_1 &= (y_1 - y_0)/l_1, \\ \theta_2 &= (y_2 - y_1)/l'_2, \\ \theta_3 &= (y_3 - (y_2 + \theta_2(l_2 - l'_2)))/l_3, \\ \theta_4 &= (y_4 - y_3)/l_4, \\ m_1 g(\theta_1 - \theta_2) + m_2 g(\theta_1 - \lambda\theta_2 + (\lambda - 1)\theta_3) - I_{x1}\ddot{\theta}_2/l'_2 + 2\gamma_1 m_1 l_1 \dot{\theta}_1 &= 0, \\ m_1 g\theta_2 + m_2 g\lambda(\theta_2 - \theta_3) + m_1 \ddot{y}_2 + I_{x1}\ddot{\theta}_2/l'_2 + 2\gamma_2 m_1 l'_2 \dot{\theta}_2 &= 0, \\ m_2 g(\theta_3 - \theta_4) - I_{x2}\ddot{\theta}_4/l_4 + 2\gamma_3 m_2 l_3 \dot{\theta}_3 &= 0, \\ m_2 g\theta_4 + m_2 \ddot{y}_4 + I_{x2}\ddot{\theta}_4/l_4 + 2\gamma_4 m_2 l_4 \dot{\theta}_4 &= 0, \end{aligned} \quad (5)$$

where the superscripts p and m for the parameters in Fig. 2 are omitted for short, g is the local gravitational acceleration, $\lambda = l_2/l'_2$ is the length ratio, γ_i are the damping factors for the motions of θ_i due to the eddy current loss of the magnetic damper, which associated with the quality factors Q_{si} and the natural angular frequencies ω_{0i} that $Q_{si} = \omega_{0i}/(2\gamma_i)$ for each degree of freedom.

The transfer function $H_y(\omega) \equiv y_4(\omega)/y_0(\omega)$ derived from Eq. (5) is used to calculate the separation fluctuation between the pendulum and the membrane caused by the horizontal seismic translational vibration, that $\Delta s(\omega) \equiv y_4^p(\omega) - y_4^m(\omega) = y_0(\omega)[H_y^p(\omega) - H_y^m(\omega)]$. The transfer function from the seismic translational motion to the separation fluctuation is defined as $H_{\Delta y}(\omega) \equiv H_y^p(\omega) - H_y^m(\omega)$. In particular, when the membrane is fixed, $y_4^m(\omega)$ is equal to $y_0(\omega)$, namely $H_y^m(\omega) = 1$.

In addition, the tilt variation of the apparatus, which may due to the ground tilt or the deformation of the vacuum chamber, can generate additional displacements y_0^p and y_0^m for the suspension points. The tilt signal $\theta_0(\omega)$ was measured by a tiltmeter fixed near the bottom of the vacuum chamber. The height from the bottom of the chamber to the suspension points are h_p and h_m for the torsion pendulum and the membrane, respectively. When the membrane is suspended as the torsion pendulum, we have $h_m = h_p$, and $y_0^p(\omega) = y_0^m(\omega) = h_p\theta_0(\omega)$. When the membrane is fixed, we have $h_m \approx 1/2h_p$, and $y_0^m(\omega) = h_m\theta_0(\omega) = 1/2h_p\theta_0(\omega)$. This coupling effect has also been observed in the ground test of the inertial sensor for LISA [37,38].

Considering these $y_0^p(\omega)$ and $y_0^m(\omega)$ as the input vibrations of Eq. (5), the separation fluctuation can be

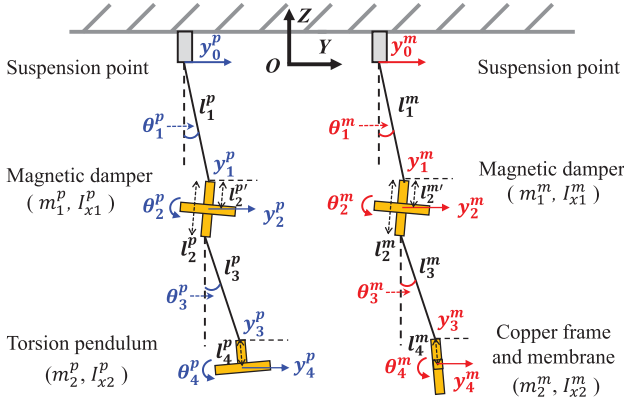


FIG. 2. Schematic of the two-stage pendulum. $O - XYZ$ is the inertial coordinate system used to relate all the position and angle parameters. The parameters y_i^j denote the small displacements deviated from the stationary positions along the separation direction, where the subscript $i = 0, 1, 2, 3, 4$, represent the different positions, and the superscript $j = p, m$ represent the subsystems for the torsion pendulum and the shielding membrane, respectively. With similar subscripts and superscripts, θ_i^j are the angles, m_i^j are the masses of each part, I_{xi}^j are the moments of inertia relative to the center of mass for each part and rotated about the x directions, l_i^j are the geometric parameters for the lengths of the fibers and the heights of the components. The motions of the suspension points y_0^p and y_0^m are assumed to be the same while driven by the environmental vibrations.

solved as $\Delta s'(\omega) \equiv y_4^p(\omega) - y_4^m(\omega) = \theta_0(\omega)[h_p H_y^p(\omega) - h_m H_y^m(\omega)]$. The tilt-separation transfer function is defined as $H'_{\Delta y}(\omega) \equiv \Delta s'(\omega)/\theta_0(\omega) = h_p H_y^p(\omega) - h_m H_y^m(\omega)$.

The transfer function $H_{\Delta y}(\omega)$ for the seismic translational motion to the separation, and $H'_{\Delta y}(\omega)$ for the tilt to the separation, are shown in Fig. 3, with the cases that the membrane is suspended and fixed to the vacuum chamber, respectively. We define the suspension lengths $l_p = \sum_{i=1}^4 l_{pi}$ and $l_m = \sum_{i=1}^4 l_{mi}$, which are the distances between the mass centers and suspension points for the torsion pendulum and the membrane, respectively. The errors of l_p and l_m can be easily achieved to ± 3 mm in the experiment. So the transfer functions with the suspended membrane are both calculated with $l_m = l_p \pm 3$ mm, while the transfer functions with $l_m = 0$ represent the fixed membrane. Under this condition, the common-mode rejection ratio (CMRR) of the separation fluctuation caused by the seismic translational motion $y_0(\omega)$ or the tilt $\theta_0(\omega)$ is at least one order of magnitude below 0.1 Hz. The CMRR increases as the length difference between l_p and l_m approaches zero.

IV. EXPERIMENTAL RESULTS

We have first performed comparative experiments with the membrane fixed and suspended, respectively. To provide clearer observation for the coupling effects of the

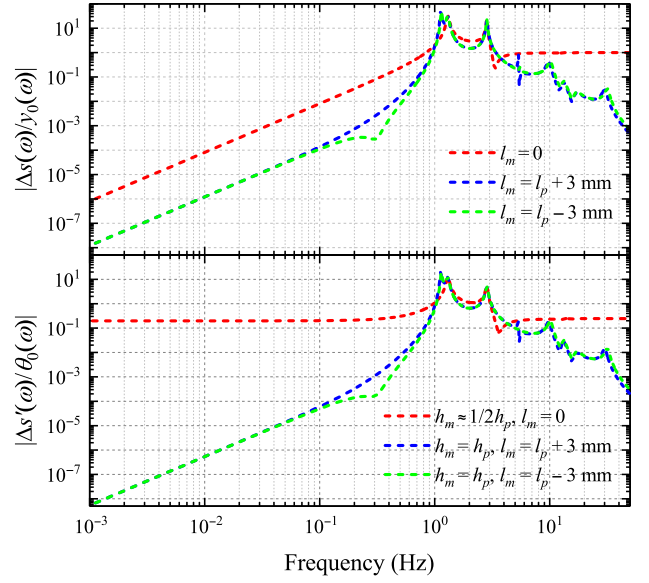


FIG. 3. The transfer functions of the separation variation $\Delta s(\omega)$ between the torsion pendulum and the membrane driven by the seismic translational motion $y_0(\omega)$ and the tilt $\theta_0(\omega)$, with different suspension lengths. The red line is calculated with the fixed membrane, while the blue and the green line are the suspended membrane with suspension length l_m equal to $l_p + 3$ mm, $l_p - 3$ mm for considering the errors of the lengths, respectively. The suspension length for the torsion pendulum is $l_p = 200$ mm. The height of the torsion-pendulum suspension point is $h_p = 443.5$ mm. The quality factors Q_{si} of all the motion modes are assumed to be 100, which affect only the transfer functions near the mode frequencies.

vibrations and the residual potential, these experiments were conducted with a larger surface potential difference between the pendulum and the membrane. Then another experiment with the membrane suspended and with a smaller surface potential difference was performed, which achieved a shorter pendulum-membrane separation of approximately $8 \mu\text{m}$.

A. Result with larger residual potential

Two comparison experiments, that with the membrane fixed and suspended, have the same residual potential difference of $\Delta U \sim 100$ mV, which is estimated by measuring the electrostatic stiffness k_e . The seismic translational motion and the tilt were recorded synchronously by a microseismograph and a tiltmeter, respectively. The electrostatic torque noise caused by the seismic translational motion and the tilt according to Eq. (4) and (5) are calculated as

$$\begin{aligned} S_{\text{seis}}^{1/2}(\omega) &= \frac{k_e}{L} S_{y_0}^{1/2}(\omega) H_{\Delta y}(\omega), \\ S_{\text{tilt}}^{1/2}(\omega) &= \frac{k_e}{L} S_{\theta_0}^{1/2}(\omega) H'_{\Delta y}(\omega), \end{aligned} \quad (6)$$

TABLE I. The main physical quantities of the torsion pendulum that are used in the calculation of k_e according to Eq. (2).

Parameters	Membrane fixed	Membrane suspended
k ($\times 10^{-8}$ N m/rad)	6.88(2)	6.72(2)
Q	~ 2500	~ 2500
I ($\times 10^{-5}$ kg m ²)	1.188(3)	1.188(3)
β ($\times 10^{-11}$ N m/V)	1.29(1)	1.03(2)
τ_c ($\times 10^{-17}$ N m)	224.2(1.2)	193.4(1.2)
k_e ($\times 10^{-7}$ N m/rad)	8.74(8)	9.11(20)
U_c (mV)	1.92(16)	1.54(5)
k_p (V/ μ rad)	0.07	0.095
k_i (V/ μ rad/s)	0.0002	0.0004
k_d (V s/ μ rad)	0.2	0.24

where $S_{y_0}^{1/2}(\omega)$, $S_{\theta_0}^{1/2}(\omega)$ are the PSDs of the measured ground translational motion and apparatus tilt, respectively.

The parameters of the torsion pendulum are summarized in Table I, including the gravitational calibration torque τ_c and its corresponding feedback voltage U_c , the PID parameters k_p , k_i , k_d , the electrostatic stiffness k_e calculated according to Eq. (2) and so on. The quality factors of the swing mode are obtained by fitting the swing angle as exponentially decaying with time when we slightly strike the vacuum chamber and giving $Q_{si}^p \sim 9$ and $Q_{si}^m \sim 36$ for the pendulum and the membrane, respectively.

The typical torque PSDs measured at the pendulum-membrane separation 22 μ m are shown in Fig. 4, with both the membrane fixed and suspended, respectively. Seismic translational motion and instrument tilt were recorded synchronously, with each data run lasting approximately 24 h.

When the membrane is fixed, the torque noise is obviously larger. The theoretical torque noise, calculated according to the measured environment vibrations, are in good agreement with the measured torque noise. This indicates that the coupling effect of environmental vibrations to the residual electrostatic force is the main noise source in the short-range ISL experiment. For comparison, the sensitivity of the torsion pendulum at the same separation of 22 μ m can be improved to reach the readout noise limit by suspending the membrane, with the improvement factor larger than 3.

B. Results with smaller residual potential

To further reduce the electrostatic related noise, we performed the experiment adopting the suspended membrane with smaller residual potential difference ($\Delta U \sim 30$ mV), by recoating the membrane with a layer of gold. Several typical measured torque PSDs at different separations are

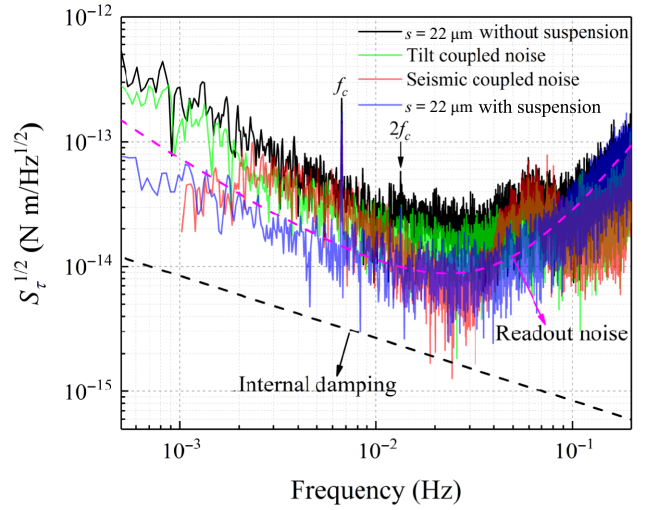


FIG. 4. Typical torque PSDs of the torsion pendulum with 22 μ m of pendulum-membrane separation under larger residual potential difference. The black, blue lines are the measured torque spectra with the membrane fixed and suspended, respectively. Considering the fixed membrane, the green, red lines are the tilt coupled noise $S_{\tau_{\text{tilt}}}^{1/2}$ and the seismic translational motion coupled noise $S_{\tau_{\text{seis}}}^{1/2}$ calculated from the synchronously collected data. The readout noise (purple dashed line) agrees with the measured torque PSD (blue line), indicating that it is dominant when the membrane is suspended. The recorded seismic spectrum is attenuated below 3 mHz due to the limited measuring bandwidth of the microseismograph. The internal damping of the fiber is calculated with $Q \sim 2500$. The gravitational calibration signal is clearly observed at $f_c \sim 6.7$ mHz.

presented in Fig. 5. The torque noise below tens of millihertz increases rapidly as the pendulum-membrane separation decreases. The torque noise at the separation of $s \geq 20$ μ m has reached the internal damping noise level, which is about 3×10^{-15} N m/ $\sqrt{\text{Hz}}$ at approximately 20 mHz, while the noise at $s = 8$ μ m is about 10 times larger than that at $s \geq 20$ μ m.

The reduction on ΔU has effectively reduced the electrostatic interaction, which is critical for allowing us to collect data at minimum separations down to 8 μ m. The smaller residual potential difference decreases the electrostatic stiffness k_e , then reduces the requirement for the autocollimator readout noise, so that the sensitivity of the torsion pendulum can reach the internal damping level at separations down to 20 μ m.

At the separation of few microns, both the Casimir force due to the zero-point electromagnetic fluctuations and the residual gas damping caused by the collisions of the molecules in the gap can potentially increase the noise. These two effects have been extensively studied in the short-range force measurements [22–32] as well as the gravitational wave detectors [42–46]. We estimated them

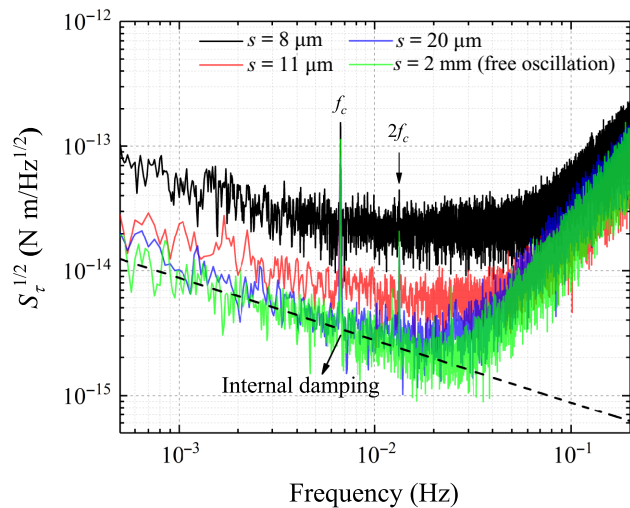


FIG. 5. The typical torque PSDs measured at different separations with smaller residual potential. The electrostatic stiffnesses obtained at the separation of $s = 8, 11, 20 \mu\text{m}$ are $(7.71 \pm 0.12), (2.53 \pm 0.03), (0.70 \pm 0.01) \times 10^{-7} \text{ N m/rad}$, respectively.

in our shortest achievable separation of approximately $8 \mu\text{m}$, and found that neither of them is significant.

The theoretical Casimir force between two perfectly conducting plates is parameterized as $F_C = \pi^2 A \hbar c / (240 s^4)$ [47], with \hbar and c denoting the reduced Planck constant and the speed of light, respectively. The Casimir force acting on the pendulum is calculated to be approximately $7.9 \times 10^{-12} \text{ N}$, which is roughly 200 times smaller than the theoretical electrostatic force $F_e \equiv \frac{1}{2} \epsilon_0 A \Delta U^2 / s^2 = 1.6 \times 10^{-9} \text{ N}$ with $\Delta U = 30 \text{ mV}$. It requires a separation of approximately $0.6 \mu\text{m}$ for the Casimir force to be comparable to the electrostatic force with $\Delta U = 30 \text{ mV}$.

The torque noise resulting from the residual gas damping at small separations can be expressed as $S_{\tau_{\text{squeeze}}}^{1/2} = \sqrt{p L^2 (8\pi k_B m_{\text{eq}} T)^{1/2} A \frac{A/\pi}{s^2 \ln[1+A/(\pi s^2)]}}$ [44], where the Boltzmann constant $k_B = 1.38 \times 10^{-23} \text{ J/K}$, the temperature $T \sim 300 \text{ K}$, the residual gas pressure $p \sim 1 \times 10^{-5} \text{ Pa}$ and the equivalent molecular weight $m_{\text{eq}} \sim 18 \text{ amu}$ [46]. The upper limit of this effect is estimated to be $S_{\tau_{\text{squeeze}}}^{1/2} \sim 6 \times 10^{-16} \text{ N m/Hz}^{1/2}$, which is roughly 50 times smaller than our lowest detected noise level of approximately $3 \times 10^{-14} \text{ N m/Hz}^{1/2}$ around 20 mHz at $s = 8 \mu\text{m}$.

V. SUMMARY AND DISCUSSION

We have built a torsion pendulum apparatus with both the fixed and the suspended membrane to verify the coupling effect of the environmental vibrations to the residual electrostatic torque in the short range. These coupling torque noises have been suppressed to below the read-out noise limit by suspending the membrane, with an

improvement factor larger than 3 for the total measured torque noise. By reducing the residual potential difference, we have improved the sensitivity of the torsion pendulum to the internal damping torque noise level with the pendulum-membrane separations down to $20 \mu\text{m}$. The shortest achievable separation is $8 \mu\text{m}$ with an acceptable noise level of approximately $3 \times 10^{-14} \text{ N m}/\sqrt{\text{Hz}}$.

Our results provide a solution for the vibration isolation in the short-range ISL test by using a torsion pendulum, and has great potential for improving the constraint of the violation of the ISL tests.

ACKNOWLEDGMENTS

This work is supported by the National Key R&D Program of China (Grant No. 2020YFC2200500), the National Natural Science Foundation of China under Grants No. 12150012, No. 12175317, No. 12005308.

- [1] S. Dimopoulos and G. Giudice, Macroscopic forces from supersymmetry, *Phys. Lett. B* **379**, 105 (1996).
- [2] N. Arkani-Hamed, S. Dimopoulos, and G. Dvali, The hierarchy problem and new dimensions at a millimeter, *Phys. Lett. B* **429**, 263 (1998).
- [3] N. Arkani-Hamed, S. Dimopoulos, and G. Dvali, Phenomenology, astrophysics, and cosmology of theories with submillimeter dimensions and TeV scale quantum gravity, *Phys. Rev. D* **59**, 086004 (1999).
- [4] L. Randall and R. Sundrum, An alternative to compactification, *Phys. Rev. Lett.* **83**, 4690 (1999).
- [5] D. B. Kaplan and M. B. Wise, Couplings of a light dilaton and violations of the equivalence principle, *J. High Energy Phys.* **2000**, 037 (2000).
- [6] N. Arkani-Hamed, S. Dimopoulos, G. Dvali, and N. Kaloper, Infinitely large new dimensions, *Phys. Rev. Lett.* **84**, 586 (2000).
- [7] R. Sundrum, Fat gravitons, the cosmological constant and submillimeter tests, *Phys. Rev. D* **69**, 044014 (2004).
- [8] E. G. Adelberger, B. R. Heckel, S. Hoedl, C. D. Hoyle, D. J. Kapner, and A. Upadhye, Particle-physics implications of a recent test of the gravitational inverse-square law, *Phys. Rev. Lett.* **98**, 131104 (2007).
- [9] J. K. Hoskins, R. D. Newman, R. Spero, and J. Schultz, Experimental tests of the gravitational inverse-square law for mass separations from 2 to 105 cm, *Phys. Rev. D* **32**, 3084 (1985).
- [10] C. D. Hoyle, U. Schmidt, B. R. Heckel, E. G. Adelberger, J. H. Gundlach, D. J. Kapner, and H. E. Swanson, Submillimeter test of the gravitational inverse-square law: A search for “large” extra dimensions, *Phys. Rev. Lett.* **86**, 1418 (2001).
- [11] C. D. Hoyle, D. J. Kapner, B. R. Heckel, E. G. Adelberger, J. H. Gundlach, U. Schmidt, and H. E. Swanson, Submillimeter tests of the gravitational inverse-square law, *Phys. Rev. D* **70**, 042004 (2004).
- [12] D. J. Kapner, T. S. Cook, E. G. Adelberger, J. H. Gundlach, B. R. Heckel, C. D. Hoyle, and H. E. Swanson, Tests of

- the gravitational inverse-square law below the dark-energy length scale, *Phys. Rev. Lett.* **98**, 021101 (2007).
- [13] L.-C. Tu, S.-G. Guan, J. Luo, C.-G. Shao, and L.-X. Liu, Null test of Newtonian inverse-square law at submillimeter range with a dual-modulation torsion pendulum, *Phys. Rev. Lett.* **98**, 201101 (2007).
- [14] S.-Q. Yang, B.-F. Zhan, Q.-L. Wang, C.-G. Shao, L.-C. Tu, W.-H. Tan, and J. Luo, Test of the gravitational inverse square law at millimeter ranges, *Phys. Rev. Lett.* **108**, 081101 (2012).
- [15] W.-H. Tan, S.-Q. Yang, C.-G. Shao, J. Li, A.-B. Du, B.-F. Zhan, Q.-L. Wang, P.-S. Luo, L.-C. Tu, and J. Luo, New test of the gravitational inverse-square law at the submillimeter range with dual modulation and compensation, *Phys. Rev. Lett.* **116**, 131101 (2016).
- [16] W.-H. Tan, A.-B. Du, W.-C. Dong, S.-Q. Yang, C.-G. Shao, S.-G. Guan, Q.-L. Wang, B.-F. Zhan, P.-S. Luo, L.-C. Tu, and J. Luo, Improvement for testing the gravitational inverse-square law at the submillimeter range, *Phys. Rev. Lett.* **124**, 051301 (2020).
- [17] J. G. Lee, E. G. Adelberger, T. S. Cook, S. M. Fleischer, and B. R. Heckel, New test of the gravitational $1/r^2$ law at separations down to 52 μm , *Phys. Rev. Lett.* **124**, 101101 (2020).
- [18] C. C. Speake and C. Trenkel, Forces between conducting surfaces due to spatial variations of surface potential, *Phys. Rev. Lett.* **90**, 160403 (2003).
- [19] W. J. Kim, A. O. Sushkov, D. A. R. Dalvit, and S. K. Lamoreaux, Surface contact potential patches and Casimir force measurements, *Phys. Rev. A* **81**, 022505 (2010).
- [20] R. O. Behunin, F. Intravaia, D. A. R. Dalvit, P. A. Maia Neto, and S. Reynaud, Modeling electrostatic patch effects in Casimir force measurements, *Phys. Rev. A* **85**, 012504 (2012).
- [21] J. Ke, W.-C. Dong, S.-H. Huang, Y.-J. Tan, W.-H. Tan, S.-Q. Yang, C.-G. Shao, and J. Luo, Electrostatic effect due to patch potentials between closely spaced surfaces, *Phys. Rev. D* **107**, 065009 (2023).
- [22] S. K. Lamoreaux, Demonstration of the Casimir Force in the 0.6 to 6 μm range, *Phys. Rev. Lett.* **78**, 5 (1997).
- [23] G. Bressi, G. Carugno, R. Onofrio, and G. Ruoso, Measurement of the Casimir force between parallel metallic surfaces, *Phys. Rev. Lett.* **88**, 041804 (2002).
- [24] W. J. Kim, M. Brown-Hayes, D. A. R. Dalvit, J. H. Brownell, and R. Onofrio, Anomalies in electrostatic calibrations for the measurement of the Casimir force in a sphere-plane geometry, *Phys. Rev. A* **78**, 020101 (2008).
- [25] G. Rajalakshmi, Torsion balance investigation of the Casimir effect. arXiv preprint arXiv: **0805**, 1183 (2008).
- [26] R. S. Decca, E. Fischbach, G. L. Klimchitskaya, D. E. Krause, D. López, U. Mohideen, and V. M. Mostepanenko, Comment on “Anomalies in electrostatic calibrations for the measurement of the Casimir force in a sphere-plane geometry”, *Phys. Rev. A* **79**, 026101 (2009).
- [27] W. J. Kim, M. Brown-Hayes, D. A. R. Dalvit, J. H. Brownell, and R. Onofrio, Reply to “Comment on ‘Anomalies in electrostatic calibrations for the measurement of the Casimir force in a sphere-plane geometry’”, *Phys. Rev. A* **79**, 026102 (2009).
- [28] W. J. Kim, A. O. Sushkov, D. A. R. Dalvit, and S. K. Lamoreaux, Measurement of the short-range attractive force between Ge plates using a torsion balance, *Phys. Rev. Lett.* **103**, 060401 (2009).
- [29] M. Masuda and M. Sasaki, Limits on nonstandard forces in the submicrometer range, *Phys. Rev. Lett.* **102**, 171101 (2009).
- [30] A. O. Sushkov, W. J. Kim, D. A. R. Dalvit, and S. K. Lamoreaux, New experimental limits on non-Newtonian forces in the micrometer range, *Phys. Rev. Lett.* **107**, 171101 (2011).
- [31] T. Graveson, C. Rackson, and W. J. Kim, Development of a high-sensitivity torsion balance to investigate the thermal Casimir force, *International Journal of Modern Physics: Conference Series. World Scientific Publishing Company* **14**, 337 (2012).
- [32] Y.-J. Chen, W. K. Tham, D. E. Krause, D. López, E. Fischbach, and R. S. Decca, Stronger limits on hypothetical Yukawa interactions in the 30–8000 nm range, *Phys. Rev. Lett.* **116**, 221102 (2016).
- [33] D. Ugolini, R. Amin, G. Harry *et al.*, Charging issues in LIGO, *International Cosmic Ray Conference*, **3**, 1283 (2008).
- [34] B. P. Abbott, R. Abbott, R. Adhikari *et al.*, LIGO: The Laser Interferometer Gravitational-Wave Observatory, *Rep. Prog. Phys.* **72**, 076901 (2009).
- [35] S. E. Pollack, M. D. Turner, S. Schlamminger, C. A. Hagedorn, and J. H. Gundlach, Charge management for gravitational-wave observatories using UV LEDs, *Phys. Rev. D* **81**, 021101 (2010).
- [36] The LIGO Scientific Collaboration, *et al.*, Advanced LIGO, *Class. Quantum Grav.* **32**, 074001 (2015).
- [37] S. K. Lamoreaux, Achieving geodetic motion for LISA test masses: Ground testing results, *Phys. Rev. Lett.* **91**, 151101 (2003).
- [38] L. Carbone, A. Cavalleri, R. Dolesi, C. D. Hoyle, M. Hueller, S. Vitale, and W. J. Weber, Upper limits on stray force noise for LISA, *Classical and Quantum Gravity* **21**, S611 (2004).
- [39] S. E. Pollack, S. Schlamminger, and J. H. Gundlach, Temporal extent of surface potentials between closely spaced metals, *Phys. Rev. Lett.* **101**, 071101 (2008).
- [40] M. Armano, H. Audley, G. Auger *et al.*, the LISA Pathfinder Collaboration, Charge-induced force noise on free-falling test masses: Results from LISA Pathfinder, *Phys. Rev. Lett.* **118**, 171101 (2017).
- [41] D. Y. Tan, L. Liu, M. Hu, and Z. B. Zhou, Seismic noise effect reduction improvement for ground-based investigation of space inertial sensor by suspending the electrode housing with an individual pendulum, *Classical Quantum Gravity* **39**, 075029 (2022).
- [42] A. Cavalleri, G. Ciani, R. Dolesi, A. Heptonstall, M. Hueller, D. Nicolodi, S. Rowan, D. Tombolato, S. Vitale, P. J. Wass, and W. J. Weber, Increased Brownian force noise from molecular impacts in a constrained volume, *Phys. Rev. Lett.* **103**, 140601 (2009).
- [43] S. Schlamminger, C. A. Hagedorn, and J. H. Gundlach, Indirect evidence for Lévy walks in squeeze film damping, *Phys. Rev. Lett.* **81**, 123008 (2010).

- [44] R. Dolesi, M. Hueller, D. Nicolodi, D. Tombolato, S. Vitale, P. J. Wass, W. J. Weber, M. Evans, P. Fritschel, R. Weiss, J. H. Gundlach, C. A. Hagedorn, S. Schlamminger, G. Ciani, and A. Cavalleri, Brownian force noise from molecular collisions and the sensitivity of advanced gravitational wave observatories, *Phys. Rev. D* **84**, 063007 (2011).
- [45] Jiao-Jiao Mao, Yu-Jie Tan, Jian-Ping Liu, Shan-Qing Yang, Jie Luo, Cheng-Gang Shao, and Ze-Bing Zhou, Residual gas damping noise in constrained volume in space-borne gravitational wave detection, *Classical Quantum Gravity* **40**, 075015 (2023).
- [46] Yu-Jie Zhao, Gui-Lin Li, Li Liu, Cheng-Gang Shao, Ding-Yin Tan, Hang Yin, and Ze-Bing Zhou, Experimental verification of and physical interpretation for adsorption-dependent squeeze-film damping, *Phys. Rev. Appl.* **19**, 044005 (2023).
- [47] H. B. G. Casimir, On the attraction between two perfectly conducting plates, *Proc. Kon. Ned. Akad. Wet.* **51**, 793 (1948).